NANO LETTERS

Letter

pubs.acs.org/NanoLett

Magic-Number Gold Nanoclusters with Diameters from 1 to 3.5 nm: Relative Stability and Catalytic Activity for CO Oxidation

Hui Li,[†,‡,¶] Lei Li,[‡,¶] Andreas Pedersen,[§,¶] Yi Gao,[∥] Navneet Khetrapal,[‡] Hannes Jónsson,[*,§,⊥] and Xiao Cheng Zeng[*,‡]

[†]Institute of Physics, Chinese Academy of Sciences, Beijing 100190, People's Republic of China

[‡]Department of Chemistry and Nebraska Center for Materials and Nanoscience, University of Nebraska—Lincoln, Lincoln, Nebraska 68588, United States

[§]Science Institute of University of Iceland, 101 Reykjavík, Iceland

[∥]Shanghai Institute of Applied Physics, Chinese Academy of Sciences, Shanghai 201800, People's Republic of China

[⊥]Department of Applied Physics, Aalto University, 02150 Espoo, Finland

ABSTRACT: Relative stability of geometric magic-number gold nanoclusters with high point-group symmetry (I_h, D_{5h}, O_h) and size up to 3.5 nm, as well as structures obtained by global optimization using an empirical potential, is investigated using density functional theory (DFT) calculations. Among high-symmetry nanoclusters, our calculations suggest that from Au(147) to Au(923), the stability follows the order $I_h > D_{5h} > O_h$. However, at the largest size of Au(923), the computed cohesive energy differences among high-symmetry I_h, D_{5h} and O_h isomers are less than 4 meV/atom (at PBE level of theory), suggesting the larger high-symmetry clusters are similar in stability. This conclusion supports a recent experimental demonstration of controlling morphologies of high-symmetry Au(923) clusters (Plant, S. R.; Cao, L.; Palmer, R. E. *J. Am. Chem. Soc.* **2014**, *136*, 7559). Moreover, at and beyond the size of Au(549), the face-centered cubic-(FCC)-based structure appears to be slightly more stable than the I_h structure with comparable size, consistent with experimental observations. Also, for the Au clusters with the size below or near Au(561), reconstructed icosahedral and decahedral clusters with lower symmetry are slightly more stable than the corresponding high-symmetry isomers. Catalytic activities of both high-symmetry and reconstructed I_h-Au(147) and both I_h-Au(309) clusters are examined. CO adsorption on Au(309) exhibits less sensitivity on the edge and vertex sites compared to Au(147), whereas the CO/O_2 coadsorption is still energetically favorable on both gold nanoclusters. Computed activation barriers for CO oxidation are typically around 0.2 eV, suggesting that the gold nanoclusters of ~2 nm in size are highly effective catalysts for CO oxidation.

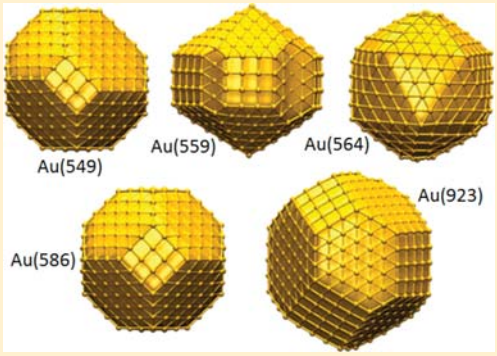

KEYWORDS: *gold nanoclusters, magic number, relative stability, surface reconstruction, CO oxidation*

Gold nanoclusters have attracted much attention over the past two decades largely owing to their high potential in chemical, biomedical, and plasmonics applications.[1] Although bulk gold is chemically inert, gold nanoclusters and nanoparticles can exhibit exceptional catalytic activity toward a number of important chemical reactions, such as CO oxidation, hydrogenation, dehydrogenation, and selective oxidation.[2−23] A particularly interesting aspect is the effect of cluster size on chemical and physical properties.[9] For example, gold nanoclusters with different sizes can show markedly different electronic structures and activities, thereby giving size- and site-dependent activation barriers and reaction rates. In addition, a main topic in cluster science is to understand structure evolution of clusters versus their size, and how chemical and physical properties of clusters evolve from small to large size and ultimately to the bulk limit.[24]

To date, the atomic structure of gold anion clusters Au_N^- in the size range of N = 3−20 (or 0.3−0.5 nm) have been well established via numerous joint experimental and theoretical studies.[25−39] Notably, the anion clusters Au_3^-−Au_{11}^- exhibit two-dimensional (2D) planar structures, Au_{13}^-−Au_{15}^- possess shell-like flat cage structures, Au_{16}^-−Au_{18}^- possess hollow-cage structures, and Au_{18}^-−Au_{20}^- possess compact pyramidal structures (golden pyramids). The hollow cage-to-pyramidal structure transition occurs at Au_{18}^- as both the cage and pyramidal isomers coexist in the cluster beam.[36] In the size range of $21 \leq N \leq 24$, hollow tubular structures become energetically more competitive than the pyramid-like structures.[40] Au_{25}^- appears to be the smallest gold cluster to exhibit a core−shell structure with a single atom core and 24-atom shell,[40] likewise Au_{26}^-−Au_{28}^-, and Au_{30}^- also possess a one-atom core.[35,41] Although neutral Au_{32} was predicted to exhibit

Received: November 1, 2014
Revised: November 26, 2014
Published: December 10, 2014

an icosahedral cage structure,[42] several studies show that anionic Au_{32}^- possesses a core−shell structure.[41,43−45] We previously reported that Au_{32}^- features a three-atom triangular core, whereas Au_{33}^- to Au_{38}^- all contain a four-atom tetrahedral core. The tetrahedral Au_4 core is a highly robust motif for low-lying medium-sized gold structures.[41,46] More recently, Jiang and Walter predicted that the electronic magic-cluster Au_{40} exhibits a twisted pyramidal core−shell structure with the Au_4 tetrahedral core as well. If this pyramidal core−shell structure is confirmed experimentally, it would show that the tetrahedral Au_4 core can survive within an unusually large size range, possibly from Au_{33}^- to Au_{40}^-. Beyond Au_{50}^-, determination of atomic structures of gold clusters becomes increasingly challenging because, similar to Au_{26}^-, Au_{29}^-, and Au_{31}^-, many medium-sized gold clusters have two or more coexisting isomers in the cluster beam.[35,41] Wang, Gong, and co-workers previously predicted that the electronic magic-number (i.e., shell-closing) Au_{58}^- cluster exhibits a core−shell structure with an Au_{12} core.[47]

It is known that clusters with certain special numbers of atoms are much more abundant than others when generated in typical cluster experiments, and these numbers are called geometric "magic numbers".[48] For nanoclusters of close-packed metals, the geometric magic numbers normally are 13, 55, 147, 309, 561, and 923 corresponding to highly symmetric structures such as icosahedral, Ino-decahedral, and cuboctahedral, with I_h, D_{5h}, and O_h symmetries, respectively (see Figure 1). The magic

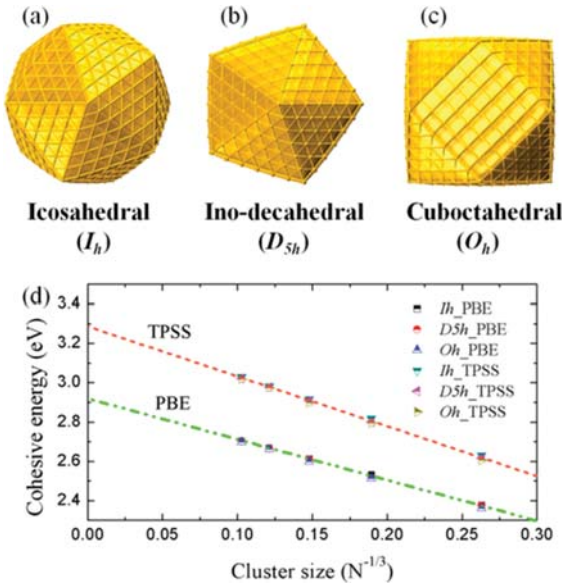

Figure 1. Optimized Structures at the PBE level of DFT method of (a) icosahedral (I_h), (b) Ino-decahedral (D_{5h}), and (c) cuboctahedral (O_h) Au_{923} clusters. (d) Cohesive energies of gold clusters versus $N^{-1/3}$.

numbers coincide with the closure of 1, 2, 3, 4, 5, and 6 shells, respectively. The I_h and D_{5h} structures are commonly observed in nanoparticles, whereas their 5-fold symmetry is prohibited in crystals by the crystallographic translational-symmetry rules.[48] Magic-number gold nanoclusters can exhibit special properties. For example, it has been suggested that the Au(55) cluster is a superior oxidation catalyst due to large oxidation resistance.[49,50]

Density functional theory (DFT) methods have been widely used to study structural, chemical, and physical properties of gold clusters. For gold nanoclusters in the size range of 1−1.7 nm, Häberlen et al. performed scalar relativistic DFT calculations of several icosahedral, octahedral, and cuboctahedral clusters with size up to Au(147). They showed that the cohesive energy and other physical properties converge linearly toward those of the bulk with increasing cluster size.[51] Another DFT study by Barnard et al. showed that among the geometric magic clusters with size <1 nm, the most stable one exhibits the cuboctahedral geometry, but as the size gradually increases to 1.7 nm, they exhibit truncated octahedral, octahedral, and truncated cube structures, respectively.[24] Pei et al. performed a DFT-based basin-hopping search of low-energy structures of Au(55) clusters and found that a disordered lowest-energy structure is 0.47 eV lower in energy than the high-symmetry I_h Au(55) isomer.[52] Both DFT and empirical model calculations suggest that the icosahedral structure is more stable than either Ino-decahedral or cuboctahedral structures for Au(147), with the stabilities of icosahedron > Ino-decahedron > cuboctahedron at this size.

Numerous experimental studies of the structure of gold nanoclusters with size >1 nm have been reported. For instance, the X-ray powder diffraction analysis by Cleveland et al. suggests the truncated−decahedral motif in three classes of gold nanoclusters with sizes of 1−2 nm.[53] Wang and Palmer studied dynamical behavior of size-selected Au(55) clusters using scanning transmission electron microscopy (STEM), and they found that Au(55) clusters exhibit chiral-type structure rather than high-symmetry structures.[54] Koga et al. studied larger gold nanoclusters of 2−3 nm and drew similar conclusions.[55] Later, the transition from the icosahedral to decahedral morphology was resolved from high-resolution electron microscopy (HREM) measurement for gold nanoparticles with size 3−14 nm.[56] The STEM studies indicate that the Au(309 ± 6) clusters have similar stabilities among Ino-decahedral, cuboctahedral, and icosahedral structures, as the three distinct structures can be detected by high−angle annular dark field (HAADF) detectors.[57,58] Another HAADF-STEM study on larger Au(923 ± 23) clusters shows that I_h structures undergo structural transformations to decahedral (D_h) or FCC isomers after electron radiation, indicating the FCC structure is already thermodynamically more stable than the I_h structure.[59] On the other hand, theoretical calculations based on the Gupta empirical potential also predict relative stability of gold clusters changing with the number of atoms.[57,58] In the range of N = 500−1000, the stability rankings are predicted to be Ino-decahedral < icosahedral < cuboctahedral, and the rankings become cuboctahedral < Ino-decahedral < icosahedral for N > 1000.[57] Barnard et al. predicted that gold nanoparticles with size >3 nm favor a modified truncated octahedral structure. Their prediction was on the basis of a shape-dependent thermodynamics model combined with surface energies obtained from a slab model.[60] However, to our best knowledge, first−principles calculations of relative stabilities of gold nanoclusters with size >2 nm have not been reported in the literature largely due to high computing costs. With the recent development of linear scaling DFT methods and more powerful computers, first-principles calculations of gold clusters up to 1000 atoms are feasible.

The strong structure−size−property relationship for the gold nanoclusters is manifested in their catalytic activity as a function of the size of clusters. In a previous review, Nørskov et al. summarized from many early experiments[61−71] that the gold nanoclusters with size <3−5 nm are most active, whereas the nanoclusters with size >10 nm are generally inert to most

dx.doi.org/10.1021/nl504192u | Nano Lett. 2015, 15, 682−688

chemical reaction.[72] The high catalytic activity of gold nanoclusters is largely attributed to the existence of low-coordinated gold atoms, such as the corner and edge sites. More recent experiments confirm unequivocally the important role played by the corner and edge sites of gold nanoclusters in CO oxidation.[70] Several recent theoretical studies also pointed out the importance of the low-coordinated sites and the protrusive sites in subnanometer gold nanoclusters to the high activity for CO oxidation.[73,74] For gold nanoclusters beyond 1 nm, both the chemical and the structural environment of gold atoms is expected to be different from that of subnanometer clusters. Hence, it is of fundamental importance to investigate catalytic activity of gold nanoclusters with size >1 nm.[75,76]

In this Letter, we employ DFT methods to study relative stability of magic-number gold nanoclusters with icosahedral, Ino-decahedral, and cuboctahedral structures in the range of 1.1−3.5 nm (containing 2−7 atomic shells of 55−923 atoms). In addition, the structures of global minima for Au(147) and Au(309) clusters (Figure 2a−c) determined based on the

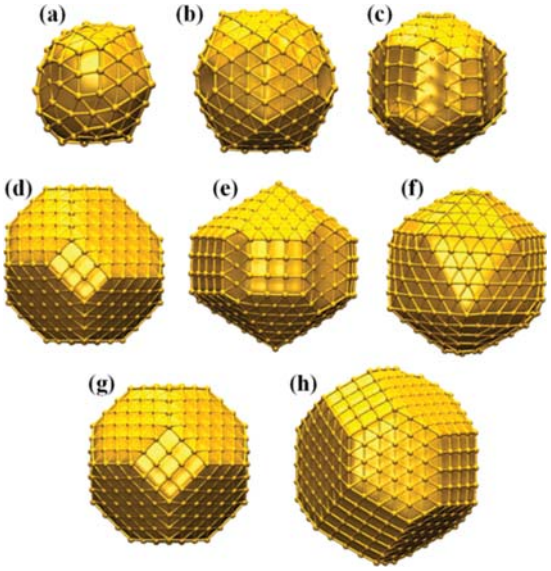

Figure 2. Structures of (a) the icosahedra-like global minimum of Au(147) (Rec-Ico-Au(147)) based on a global optimization with the EMT potential, (b) the reconstructed icosahedral Au(309) (Rec-Ico-Au(309)), (c) the reconstructed decahedral Au(309) (Rec-Dec-Au(309)), (d) the FCC Au(549), (e) the decahedral Au(559), (f) the reconstructed icosahedral Au(564) (Rec-Ico-Au(564)), (g) the truncated octahedral (TO) Au(586), and (h) the FCC Au(923) cluster determined in ref 59.

global optimization using saddle traversals (GOUST) scheme[77] coupled with an effective−medium−theory (EMT) potential are also examined. Both clusters can be viewed as reconstructed structures from the corresponding icosahedral or decahedral motif, as shown in Figure 2a−c. For convenience, the reconstructed icosahedral and decahedral structures are denoted as Rec-Ico and Rec-Dec, respectively. Moreover, three highly ordered gold clusters near the magic number N = 561, that is, Au(549) based on FCC motif (Figure 2d), decahedral Au(559) (Figure 2e), and a reconstructed icosahedral Au(564) (Figure 2f), are also considered. A previous DFT study showed that the truncated octahedral gold nanocluster (or bulk FCC-like gold structure) is energetically very competitive compared to the high-symmetry icosahedral and decahedral structures. Hence, we also compute cohesive energy of a truncated octahedral Au(586) (Figure 2g). Lastly, an FCC isomer of the Au(923) determined experimentally in ref 59. (Figure 2h) is considered for comparison.

Specifically, we use the QUICKSTEP program implemented in the CP2K software package.[78,79] The generalized gradient approximation (GGA) in the form of Perdew−Burke−Ernzerhof (PBE)[80] is selected, and the core electrons of gold atom are described by the Goedecker−Teter−Hutter (GTH)[81,82] norm-conserving pseudopotential. The basis sets are a combination of the polarized double-ζ quality Gaussian basis and a plane-wave basis set (with an energy cutoff of 280 Ry). The structures of all gold nanoclusters are fully relaxed until the maximum force on each atom is no larger than 4.5 × 10^{-4} Hatree/Bohr. The meta-GGA Tao−Perdew−Staroverov−Scuseria (TPSS)[83] functional has been proven to yield more accurate energy rankings among isomers of small gold clusters.[84] Thus, in this study, we also present computed TPSS energies of gold nanoclusters based on the geometries optimized at the PBE level of theory. Lastly, to locate the transition state of CO oxidation on gold nanoclusters, we adopt the linear and quadratic synchronous transit (LST/QST) method[85,86] at the PBE level with the double polarizable (DNP) basis set, implemented in the DMol^3 software package.[87,88] Only the CO oxidation on the medium-sized Au(147) and Au(309) clusters is investigated, due to the high computation cost for the larger gold nanoclusters.

As shown in Table 1, our DFT calculations suggest that the cohesive energies of the high-symmetry icosahedral, Ino-decahedral, and cuboctahedral structures are very close to each other. Nevertheless, the cohesive energy order of I_h > D_{5h} > O_h is still kept from Au(55) to Au(923) for the high-symmetry magic-number nanoclusters. However, for Au(561) and Au(923), the computed cohesive energy difference

Table 1. Computed Cohesive Energy[a] of Icosahedra[b], Ino-Decahedra[c], Cuboctahedra[d] Au(N)[e], Truncated Octahedra Au(586), As Well As Reconstructed Icosahedra, Decahedra, and Cuboctahedra, FCC, and Experimentally Proposed Au(923) Nanoclusters[f]

	icosahedra	decahedra	cuboctahedra FCC
Au(55)[g]	2.378 (2.632)	2.373 (2.618)	2.363 (2.607)
Au(147)	2.532 (2.818)	2.518 (2.799)	2.515 (2.796)
	2.544 (**2.822**)[h]		
Au(309)	2.612 (2.917)	2.609 (2.909)	2.600 (2.899)
	2.619 (2.920)[c1]	2.622 (**2.923**)[c2]	
Au(561)	2.667 (2.984)	2.665 (2.979)	2.662 (2.975)
Au(549−564)	2.675 (2.989)[d1]	2.676 (2.991)[d2]	2.678 (**2.992**)[d3]
Au(586)			2.685 (**3.000**)[k]
Au(923)	2.704 (3.030)	2.701 (3.023)	2.699 (3.020)
			2.713 (**3.035**)[l]

[a]In eV. [b]Denoted I_h. [c]Denoted D_{5h}. [d]Denoted O_h. [e]N = 55, 147, 309, 561, and 923. [f]Values given outside and inside parentheses are computed based on PBE and TPSS functional, respectively. [g]Disordered Au(55)[52] or chiral-type Au(55)[53] is more stable than Ico-Au(55). [h]The cohesive energy of Rec-Ico-Au(147). [i]The cohesive energy of Rec-Ico-Au(309) (c1) and Rec-Dec-Au(309) (c2). [j]Cohesive energy of Rec-Ico-Au(564) (d1), decahedral Au(559) (d2), and FCC Au(549) (d3). [k]Cohesive energy of the truncated octahedral Au(586). [l]Experimentally proposed FCC Au(923) in ref 59.

dx.doi.org/10.1021/nl504192u | Nano Lett. 2015, 15, 682−688

between I_h, D_{5h} and O_h isomers is less than 4 meV/atom (at PBE level of theory; see Table 1), suggesting the larger high-symmetry clusters are practically equally stable. This conclusion supports a recent experimental demonstration of the control of cluster morphology of high-symmetry Au(923) clusters by small changes in growth conditions.[89] Moreover, our DFT calculations show that the reconstructed icosahedral Au(147) (Rec-Ico-Au(147)) is notably more stable than the three high-symmetry isomers. For Au(309), the reconstructed decahedral structure (Rec-Dec-Au(309)) has greater cohesive energy than that of the reconstructed icosahedral counterpart. Starting from Au(549), the FCC structure becomes energetically most favorable, suggesting that gold nanoclusters already favor the FCC structure at a size of 2.2 nm. Indeed, the experimentally proposed FCC Au(923) cluster has slightly larger cohesive energy than the icosahedral isomer.

The cohesive energy per atom exhibits a linear relationship with the size of gold nanoclusters, as shown in Figure 1. The cohesive energy of I_h structures (based on the PBE and TPSS calculations) as a function of size N can be fitted to the following two relations:

$$E_c^{PBE}(I_h) = 2.913 - 2.029 \times N^{-1/3} \quad (1)$$

and

$$E_c^{TPSS}(I_h) = 3.285 - 2.478 \times N^{-1/3} \quad (2)$$

The extrapolated cohesive energy of bulk gold from eq 1 is 2.91 eV, consistent with previous PBE calculation of bulk gold.[90] The extrapolated cohesive energy of bulk gold from eq 2 (3.28 eV) is closer to the experimentally measured value (3.84 eV). As mentioned above, both PBE and TPSS calculations give rise to cohesive energy in the order of icosahedra > Ino-decahedra > cubotachedra. This ordering is contrary to the one obtained from the Gupta empirical potential, that is, $D_{5h} > I_h > O_h$ for Au(N) ($N > 500$).

At $N = 147$, the reconstructed icosahedron appears to be the most stable structure. At $N = 309$, the cohesive energy (2.622 eV via PBE, and 2.923 eV via TPSS) of reconstructed decahedral structure is already greater than the reconstructed icosahedral structure (2.619 eV via PBE, and 2.920 eV via TPSS), indicating a structure transition from reconstructed icosahedra to decahedra at $N < 309$. This conclusion is consistent with the STEM investigation of Au(309 ± 6) clusters on carbon film.[57] For the clusters whose sizes are close to $N = 561$, the FCC structure Au(549) (2.678 eV via PBE, and 2.992 eV via TPSS) has a slightly greater cohesive energy than both reconstructed icosahedral Au(564) (2.675 eV via PBE, and 2.989 eV via TPSS) and decahedral Au(559) (2.676 eV via PBE, and 2.991 eV via TPSS), indicating a structure transition from reconstructed decahedra to FCC at a size $N \sim 549$. Computed cohesive energy of the truncated octahedral Au(586) (2.685 eV via PBE, and 3.000 eV via TPSS) is also greater than interpolated energy (2.671 eV via eq 1, and 2.989 eV via eq 2) at $N = 586$, confirming that the FCC structure is more stable beyond $N \sim 549$.

To gain additional insight into the relative stability among the magic-number nanoclusters, we compute the coordination numbers and Au−Au bond lengths of all the gold nanoclusters. As shown in Figure 3a, gold atoms in either high-symmetry or reconstructed icosahedral clusters have average coordination numbers higher than those of the decahedral and cuboctahedral clusters of similar size, and their coordination numbers increase

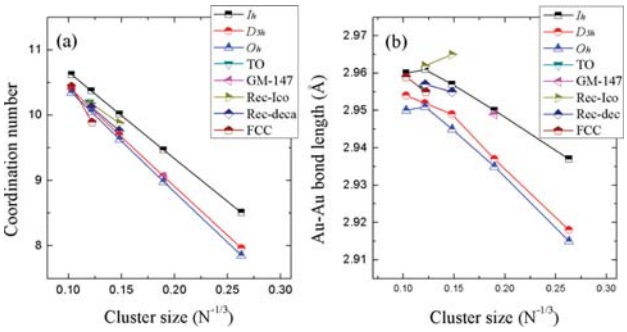

Figure 3. (a) Average coordination numbers of gold atoms and (b) nearest-neighbor Au−Au distance versus $N^{-1/3}$.

linearly with the cluster size. For the high-symmetry structures, higher coordination number likely renders the icosahedral clusters more stable than the decahedral and cuboctahedral counterparts. However, for the reconstructed structures, higher coordination number seems less important from Au(147) to Au(564). For example, the predicted global minimum of Au(147) (based on the EMT potential) almost has the same coordination number as the high-symmetry decahedral Au(147). The reconstructed icosahedral clusters of both Au(309) and Au(564) also have much lower coordination number than the I_h isomers, and the reconstructed decahedral Au(309) and Au(559) have similar coordination numbers as the D_{5h} isomers. Interestingly, the FCC Au(549), which shows the highest stability, has significantly lower coordination number than all other clusters with similar size, indicating that higher coordination number is not the only factor determining the stability of large gold clusters with size beyond 2 nm.

Unlike the trend in coordination number, the Au−Au bond lengths exhibit a nonmonotonous trend with cluster size, as shown in Figure 3b. The average bond length increases linearly with the cluster size from Au(55) to Au(561), and such a linear relation was also found in previous DFT study of Au(55) and Au(147).[50] However, this linear relation no longer holds for large clusters beyond 2 nm, and the Au−Au bond lengths decreases slightly from Au(561) to Au(923) for the I_h and O_h clusters. Such a bond contraction can also be seen from the low-lying reconstructed icosahedral Au(309) to Au(564). The Au−Au bonds in the icosahedral clusters are notably longer than those in the decahedral and cuboctahedral clusters. The reconstructed icosahedral isomers also exhibit longer Au−Au bonds than the decahedral and FCC clusters Au(309) and decahedral Au(559); the Au−Au bonds of FCC Au(549) are between the shorter bond-lengths of D_{5h} and O_h structures and longer bond-lengths of I_h structures, suggesting that highly stable, large gold clusters may favor Au−Au bond-lengths between those of the D_{5h} and I_h geometries.

In addition to relative stabilities among gold nanoclusters with different structures, we have also investigated size and shape dependence of catalytic activity by using the CO oxidation as a benchmark. First, the adsorption energy of CO and O_2 molecules on three typical (vertex, edge, and surface) sites of high-symmetry I_h-Au(147) and I_h-Au(309) clusters (see Figure 4), and atomic sites with small cone-angle[73] on Rec-Ico Au(147) and Rec-Dec Au(309) clusters are computed. As shown in Figure 4, the CO molecule can be chemisorbed on the vertex, edge and surface sites of I_h-Au(147) and I_h-Au(309) clusters, with a C−Au bond length of ~2.0 Å. The CO

dx.doi.org/10.1021/nl504192u | Nano Lett. 2015, 15, 682−688

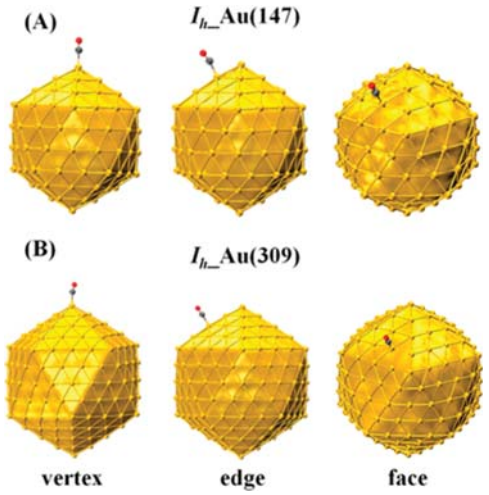

Figure 4. CO molecules adsorbed on three different sites of (A) I_h-Au(147) and (B) I_h-Au(309) nanoclusters. The adsorption energies of CO on the vertex, edge, and face sites of I_h-Au(147) (I_h-Au(309)) are −0.814 (−0.754), −0.557 (−0.578), and −0.404 (−0.463) eV, respectively.

admolecule is energetically more favorable on the vertex site (adsorption energy, E_a = 0.814 eV) than on the edge site (E_a = 0.557 eV) of I_h-Au(147). Similarly, the vertex sites of I_h-Au(309) can bind the CO molecule stronger than the edge sites, but the adsorption energy difference between vertex and edge sites is less for the larger I_h-Au(309) cluster. Also, CO adsorption is weaker on the Rec-Ico-Au(147) and Rec-Dec-Au(309) (E_a = −0.723 and −0.627 eV, respectively) compared with the corresponding Au clusters with higher symmetry, indicating structural dependence of the CO adsorption.

Our DFT calculations also show that the O_2 molecule is weakly adsorbed on Au(147) and Au(549) clusters (E_a = ∼0.080 and ∼0.135 eV, respectively). However, the O_2 adsorption can be enhanced to ∼0.155 and 0.210 eV when the O_2 is coadsorbed next to a CO molecule, a common feature reported previously for the small- and medium-sized gold clusters.[73,74] It is known that the coadsorption of CO and O_2 molecules on gold clusters can be an important factor to the efficiency of CO oxidation.

The computed reaction pathways for the CO oxidation on I_h-Au(147), and I_h-Au(309) clusters are shown in Figure 5. Here, we only consider CO adsorbed initially on a vertex site (the most active site due to low-coordination[73,91]) and O_2 on a neighboring edge site. As shown in Figure 5, CO oxidation on both high-symmetry clusters exhibit double-transition-state (DTS) pathways as commonly seen with small- and medium-sized gold clusters.[73,91] In the first step of CO oxidation, the C atom of CO attracts O_2 molecule, followed by crossing a low energy barrier (0.00 and 0.077 eV for the I_h-Au(147) and I_h-Au(309), respectively) to form the OCOO bridge-like intermediate (Figure 5). In the second step, CO grabs an O atom of O_2 to form a CO_2 molecule. This step is the rate-determining step. The energy barriers for releasing a CO_2 are 0.207 and 0.185 eV on I_h-Au(147) and I_h-Au(309), respectively. So, the barrier slightly decreases with increasing size of Au nanoclusters.

As shown in Figure 5a and b, CO oxidation on Rec-Ico-Au(147) and Rec-Ico-Au(309) entails very similar DTS pathways as the high-symmetry icosahedral counterparts. The

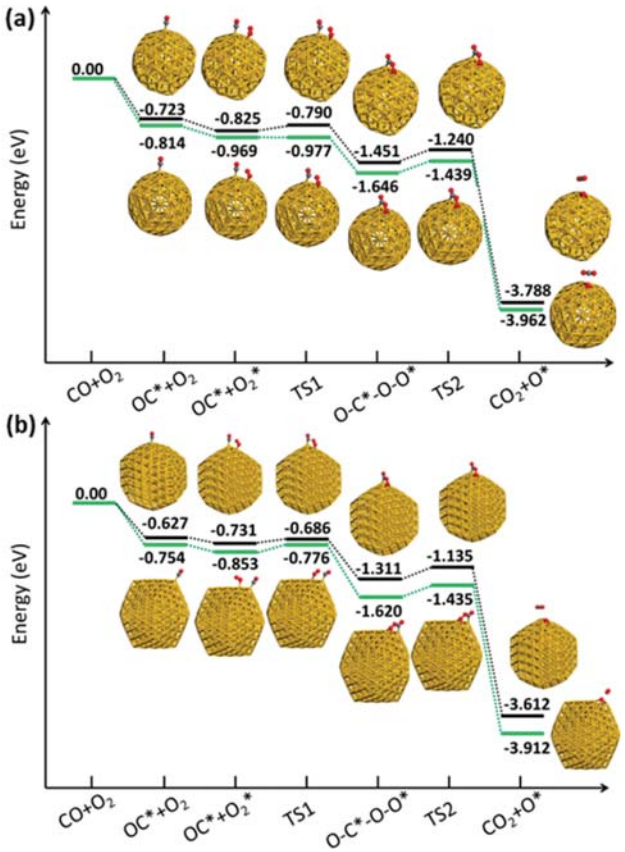

Figure 5. Computed reaction pathway for the CO oxidation on (a) I_h-Au(147) (green pathway) and Rec-Ico-Au(147) (black pathway), (b) I_h-Au(309) (green pathway) and Rec-Dec-Au(309) (black pathway), respectively. Here, the symbol * represents the adsorption of the corresponding molecules on Au atoms.

computed reaction barriers for the first and the second step are ∼0.035 (0.045) and ∼0.211 (0.176) eV for Rec-Ico-Au(147) (Rec-Ico-Au(309)), respectively, comparable with those on the high-symmetry icosahedral clusters. Hence, reconstructed structures exhibit similar catalytic activity as the high-symmetry I_h-Au(147) and I_h-Au(309) nanoclusters. In other words, for relatively larger Au nanoclusters, the symmetry plays little role in the activity for CO oxidation.

In conclusion, we have performed DFT calculations to examine relative stabilities of geometric magic-number gold nanoclusters with size up to 3.5 nm for the first time. Our calculations show that for high-symmetry clusters from Au(147) to Au(923), the cohesive energy rankings of I_h > D_{5h} > O_h are kept. However, at the size Au(309), a reconstructed decahedral cluster seems energetically slightly more favorable than the icosahedral counterpart, whereas at the size Au(549), the FCC-based structure is more stable than other geometric magic-number clusters, consistent with experimental results. At the largest size of Au(923), the computed cohesive energy differences among high-symmetry I_h, D_{5h}, and O_h isomers are less than 4 meV/atom (at PBE level of theory), suggesting the three high-symmetry clusters are very close in stability, although the FCC-based structure appears to be most stable. It is known that in the bulk limit, gold crystal exhibits FCC structure. On CO adsorption, the I_h-Au(309) exhibits less sensitivity to the vertex and edge sites compared to I_h-Au(147), suggesting that gold nanoclusters with size beyond

dx.doi.org/10.1021/nl504192u | Nano Lett. 2015, 15, 682−688

2 nm exhibit weaker site-dependent properties and catalytic activities. The mutual promotion effect of CO/O_2 coadsorption is also seen on large gold nanoclusters. Our DFT calculations show that the gold clusters from 1 to 2 nm are still highly active for CO oxidation due to the low reaction barriers (~0.2 eV). In fact, the 2 nm gold cluster entails lower reaction barrier than the 1 nm gold cluster, albeit with weaker CO and O_2 adsorption. It will be interesting to study size-dependent catalytic activities for the gold nanoclusters from 3 to 5 nm in the future.

AUTHOR INFORMATION

Corresponding Authors

*E-mail: xzeng1@unl.edu.

*E-mail: Hannes_jonsson@brown.edu.

Author Contributions

¶These authors contributed equally.

Notes

The authors declare no competing financial interest.

ACKNOWLEDGMENTS

X.C.Z. is supported by grants from ARL (W911NF1020099) and University of Nebraska-Lincoln Nebraska Center for Energy Sciences Research, and by University of Nebraska Holland Computing Center and the Center for Functional Nanomaterials (CFN) Theory and Computation Facility in Brookhaven National Laboratory (Research carried out in part at the Center for Functional Nanomaterials, Brookhaven National Laboratory, which is supported by the U.S. Department of Energy, Office of Basic Energy Sciences, under Contract No. DE-AC02-98CH10886). H.J. and A.P. are supported by Icelandic Science Fund and Academy of Finland. We thank Dr. Joel Brehm (UNL) for preparation of the high-quality images of gold nanoclusters.

REFERENCES

(1) Hutchings, G. J.; Burst, M.; Schmidbaur, H. *Chem. Soc. Rev.* **2008**, *37*, 1759.

(2) Grabow, L. C.; Mavrikakis, M. *Angew. Chem., Int. Ed.* **2008**, *47*, 7390.

(3) Daniel, M.-C.; Astruc, D. *Chem. Rev.* **2004**, *104*, 293.

(4) Hashmi, A. S. K.; Hutchings, G. J. *Angew. Chem., Int. Ed.* **2006**, *45*, 7896 and references therein..

(5) Pyykkö, P. *Angew. Chem., Int. Ed.* **2004**, *43*, 4412.

(6) Pyykkö, P. *Chem. Soc. Rev.* **2008**, *37*, 1967 and references therein..

(7) Pyykkö, P. Relativistic *Theory of Atoms and Molecules*; Springer: Berlin, 2000; Vol. *III*, pp 108−111.

(8) Schwarz, H. *Angew. Chem., Int. Ed.* **2003**, *42*, 4442.

(9) Pina, C. D.; Falletta, E.; Prati, L.; Rossi, M. *Chem. Soc. Rev.* **2008**, *37*, 2077 and references therein..

(10) Haruta, M.; Kobayashi, T.; Samo, H.; Yamada, N. *Chem. Lett.* **1987**, 405.

(11) Haruta, M.; Yamada, N.; Kobayashi, T.; Ijima, S. *Catal. Today* **1989**, *115*, 301.

(12) Haruta, M. *Catal. Today* **1997**, *36*, 115.

(13) Haruta, M. *Catal. Today* **1997**, *36*, 153.

(14) Bond, G. C. *Catal. Today* **2002**, *72*, 5.

(15) Wesendrup, R.; Hunt, T.; Schwerdtfeger, P. *J. Chem. Phys.* **2000**, *112*, 9356.

(16) Häkkinen, H.; Moseler, M.; Landman, U. *Phys. Rev. Lett.* **2002**, *89*, 033401.

(17) Hashmi, A. S. K.; Hutchings, G. J. *Angew. Chem., Int. Ed.* **2006**, *45*, 7896 and references therein..

(18) Chen, M. S.; Goodman, D. W. *Acc. Chem. Res.* **2006**, *39*, 739 and references therein..

(19) Chen, M. S.; Goodman, D. W. *Catal. Today* **2006**, *111*, 22 and references therein..

(20) Chen, M. S.; Goodman, D. W. *Chem. Soc. Rev.* **2008**, *37*, 1860 and references therein..

(21) Chen, M. S.; Goodman, D. W. *Science* **2004**, *306*, 252. 17.

(22) Bond, G. C.; Louis, C.; Thompson, D. T. *Catalysis by Gold*; Imperial College Press: London, 2006.

(23) Herzing, A. A.; Kiely, C. J.; Carley, A. F.; Landon, P.; Hutchings, G. J. *Science* **2008**, *321*, 1331.

(24) Barnard, A.; Curtiss, L. A. *ChemPhysChem* **2006**, *7*, 1544.

(25) Gruene, P.; Rayner, D. M.; Redlich, D. M.; van der Meer, A. F. G.; Lynon, J. T.; Meijer, G.; Fielicke, A. *Science* **2008**, *321*, 674.

(26) Li, J.; Li, X.; Zhai, H.-J.; Wang, L. S. *Science* **2003**, *299*, 864.

(27) Bulusu, S.; Li, X.; Wang, L. S.; Zeng, X. C. *Proc. Natl. Acad. Sci. U.S.A.* **2006**, *103*, 8326.

(28) Häkkinen, H.; Landman, U. *Phys. Rev. B* **2000**, *62*, R2287.

(29) Furche, F.; Ahlrichs, R.; Weis, P.; Jacob, C.; Glib, S.; Bierweiler, T.; Kappes, M. M. *J. Chem. Phys.* **2002**, *117*, 6982.

(30) Häkkinen, H.; Yoon, B.; Landman, U.; Li, X.; Zhai, H. J.; Wang, L. S. *J. Phys. Chem. A* **2003**, *107*, 6168.

(31) Lechtken, A.; Neiss, C.; Kappes, M. M.; Schooss, D. *Phys. Chem. Chem. Phys.* **2009**, *11*, 4344.

(32) Johansson, M. P.; Lechtken, A.; Schooss, D.; Kappes, M. M.; Furche, F. *Phys. Rev. A* **2008**, *77*, 053202.

(33) Xing, X.; Yoon, B.; Landman, U.; Parks, J. H. *Phys. Rev. B* **2006**, *74*, 165423.

(34) Yoon, B.; Koskinen, P.; Huber, B.; Kostko, O.; von Issendorff, B.; Häkkinen, H.; Moseler, M.; Landman, U. *Chem. Phys. Chem.* **2007**, *8*, 157.

(35) Schaefer, B.; Pal, R.; Khetrapal, N. S.; Amsler, M.; Sadeghi, A.; Blum, V.; Zeng, X. C.; Goedecker, S.; Wang, L. S. *ACS Nano* **2014**, *7*, 7413.

(36) Huang, W.; Bulusu, S.; Pal, R.; Zeng, X. C.; Wang, L. S. *ACS Nano* **2009**, *3*, 1225.

(37) Huang, W.; Pal, R.; Wang, L.-M.; Zeng, X. C.; Wang, L. S. *J. Chem. Phys.* **2010**, *132*, 054305.

(38) Wang, L. M.; Pal, R.; Huang, W.; Zeng, X. C.; Wang, L. S. *J. Chem. Phys.* **2010**, *132*, 114306.

(39) Pal, R.; Wang, L.-M.; Huang, W.; Wang, L. S.; Zeng, X. C. *J. Chem. Phys.* **2011**, *134*, 054306.

(40) Bulusu, S.; Li, X.; Wang, L. S.; Zeng, X. C. *J. Phys. Chem. C* **2007**, *111*, 4190.

(41) Shao, N.; Huang, W.; Gao, Y.; Wang, L. M.; Li, X.; Wang, L. S.; Zeng, X. C. *J. Am. Chem. Soc.* **2010**, *132*, 5696.

(42) Johansson, M. P.; Sundholm, D.; Vaara, J. *Angew. Chem., Int. Ed.* **2004**, *43*, 2678.

(43) Ji, M.; Gu, X.; Li, X.; Gong, X.; Li, J.; Wang, L. S. *Angew. Chem., Int. Ed.* **2005**, *44*, 7119.

(44) Jalbout, A. F.; Contreras-Torres, F. F.; Prez, L. A.; Garzn, I. L. *J. Phys. Chem. A* **2008**, *112*, 353.

(45) Johansson, M. P.; Vaara, J.; Sundholm, D. *J. Phys. Chem. C* **2008**, *112*, 19311.

(46) Shao, N.; Huang, W.; Mei, W.-N.; Wang, L. S.; Wu, Q.; Zeng, X. C. *J. Phys. Chem. C* **2014**, *118*, 6887.

(47) Huang, W.; Ji, M.; Dong, C. D.; Gu, X.; Wang, L. M.; Gong, X. G.; Wang, L. S. *ACS Nano* **2008**, *2*, 897.

(48) Teo, B. K.; Sloane, N. J. A. *Inorg. Chem.* **1985**, *24*, 4545.

(49) Turner, M.; Golovko, V. B.; Vaughan, O. P. H.; Abdulkin, P.; Berenguer-Murcia, A.; Tikhov, M. S.; Johnson, B. F. G.; Lambert, R. M. *Nature* **2008**, *454*, 981.

(50) Boyen, H.-G.; Kästle, G.; Weigl, F.; Koslowski, B.; Dietrich, C.; Ziemann, P.; Spatz, J. P.; Riethmüller, S.; Hartmann, C.; Möller, M.; Schmid, G.; Garnier, M. G.; Oelhafen, P. *Science* **2002**, *297*, 1533.

(51) Häberlen, O. D.; Chung, S.-C.; Stener, M.; Rösch, N. *J. Chem. Phys.* **1997**, *106*, 5189.

(52) Pei, Y.; Shao, N.; Gao, Y.; Zeng, X. C. *ACS Nano* **2010**, *4*, 2009.

(53) Cleveland, C. L.; Landman, U.; Schaaff, T. G.; Shafigullin, M. N.; Stephens, P. W.; Whetten, R. L. *Phys. Rev. Lett.* **1997**, *79*, 1873.

(54) Wang, Z. W.; Palmer, R. E. *Nano Lett.* **2012**, *12*, 5510.

(55) Koga, K.; Takeo, H.; Ikeda, T.; Ohshima, K. *Phys. Rev. B* **1998**, *57*, 4053.
(56) Koga, K.; Ikeshoji, T.; Sugawara, K.-I. *Phys. Rev. Lett.* **2004**, *92*, 115507.
(57) Li, Z. Y.; Young, N. P.; Vece, M. D.; Paloma, S.; Palmer, R. E.; Bleloch, A. L.; Curley, B. C.; Johnston, R. L.; Jiang, J.; Yuan, J. *Nature* **2008**, *451*, 46.
(58) Curley, B. C.; Johnston, R. L.; Young, N. P.; Li, Z. Y.; Vece, M. D.; Palmer, R. E.; Bleloch, A. L. *J. Phys. Chem. C* **2007**, *111*, 17846.
(59) Wang, Z. W.; Palmer, R. E. *Phys. Rev. Lett.* **2012**, *108*, 245502.
(60) Barnard, A. S.; Lin, X. M.; Curtiss, L. A. *J. Phys. Chem. B* **2005**, *109*, 24465.
(61) Haruta, M. *Stud. Surf. Sci. Catal.* **1997**, *110*, 123.
(62) Schimpf, S.; Lucas, M.; Mohr, C.; Rodemerck, U.; Bruckner, A.; Radnik, J.; Hofmeister, H.; Claus, P. *Catal. Today* **2002**, *72*, 63.
(63) Okumura, M.; Nakamura, S.; Tsubota, S.; Nakamura, T.; Azuma, M.; Harta, M. *Catal. Lett.* **1998**, *51*, 53.
(64) Schubert, M. M.; Hackenberg, S.; Veen, A. C.; Muhler, M.; Plzak, V.; Behm, R. *J. Catal.* **2001**, *197*, 113.
(65) Lopez, N.; Janssens, T. V. W.; Clausen, B. S.; Xu, Y.; Mavrikakis, M.; Bligaard, T.; Nøskov, J. K. *J. Catal.* **2004**, *223*, 232.
(66) Janssens, T. V. W.; Carlsson, A.; Puig-Molina, A.; Clausen, B. S. *J. Catal.* **2006**, *240*, 108.
(67) Lin, S. D.; Bollinger, M.; Vannice, M. A. *Catal. Lett.* **1993**, *17*, 245.
(68) Lee, S.-J.; Gavriilidis, A. *J. Catal.* **2002**, *206*, 305.
(69) Calla, J.; Bore, M. T.; Datye, A. K.; Davis, R. *J. Catal.* **2006**, *238*, 458.
(70) Overbury, S. H.; Schwartz, V.; Mullins, D. R.; Yan, W.; Dai, S. *J. Catal.* **2006**, *241*, 56.
(71) Yan, Z.; Chinta, S.; Mohamed, A. A.; Fackler, J. P.; Goodman, D. W. *Catal. Lett.* **2006**, *111*, 15.
(72) Hvolbæk, B.; Janssens, T. V. W.; Clausen, B. S.; Falsig, H.; Christensen, C. H.; Nøskov, J. K. *Nanotoday* **2007**, *2*, 14.
(73) Gao, Y.; Shao, N.; Pei, Y.; Chen, Z.; Zeng, X. C. *ACS Nano* **2011**, *5*, 7818.
(74) Liu, C.; Tan, Y.; Lin, S.; Li, H.; Wu, X.; Li, L.; Pei, Y.; Zeng, X. C. *J. Am. Chem. Soc.* **2013**, *135*, 2583.
(75) Janssens, T. V. W.; Clausen, B. S.; Hvolbæk, B.; Falsig, H.; Christensen, C. H.; Bligaard, T.; Nøskov, J. K. *Top. Catal.* **2007**, *44*, 15.
(76) Lopez, N.; Nøskov, J. K.; Janssens, T. V. W.; Carlsson, A.; Puig-Molina, A.; Clausen, B. S.; Grunwaldt, J.-D. *J. Catal.* **2004**, *225*, 86.
(77) Plasencia, M.; Pedersen, A.; Arnaldsson, A.; Jonsson, H. *Comput. Geosci.* **2014**, *65*, 110.
(78) VandeVondele, J.; Krack, M.; Mohamed, F.; Parrinello, M.; Chassaing, T.; Hutter. *J. Comput. Phys. Commun.* **2005**, *167*, 103.
(79) Lippert, G.; Hutter, J.; Parrinello, M. *Mol. Phys.* **1997**, *92*, 477.
(80) Perdew, J. P.; Burke, K.; Ernzerhof, M. *Phys. Rev. Lett.* **1996**, *77*, 3865.
(81) Goedecker, S.; Teter, M.; Hutter, J. *Phys. Rev. B* **1996**, *54*, 1703.
(82) Hartwigsen, C.; Goedecker, S.; Hutter, J. *Phys. Rev. B* **1998**, *58*, 3641.
(83) Tao, J.; Perdew, J. P.; Staroverov, V. N.; Scuseria, G. E. *Phys. Rev. Lett.* **2003**, *91*, 146401.
(84) Shi, Y. K.; Li, Z. H.; Fan, K.-L. *J. Phys. Chem. A* **2010**, *114*, 10297.
(85) Halgren, T. A.; Lipscomb, W. N. *Chem. Phys. Lett.* **1977**, *49*, 225.
(86) Peng, C. Y.; Schlegel, H. B. Isr. *J. Chem.* **1993**, *33*, 449.
(87) Delley, B. *J. Chem. Phys.* **1990**, *92*, 508.
(88) Delley, B. *J. Chem. Phys.* **2000**, *113*, 7756.
(89) Plant, S. R.; Cao, L.; Palmer, R. E. *J. Am. Chem. Soc.* **2014**, *136*, 7559.
(90) Jensen, P.; Blase, X.; Ordejón, P. *Surf. Sci.* **2004**, *564*, 173.
(91) Li, L.; Gao, Y.; Li, H.; Zhao, Y.; Pei, Y.; Chen, Z. F.; Zeng, X. C. *J. Am. Chem. Soc.* **2013**, *135*, 19336.